Scattering from an Open Spherical Shell Having a Circular Aperture and Enclosing a Concentric Dielectric Sphere

RICHARD W. ZIOLKOWSKI, MEMBER, IEEE, DIANE P. MARSLAND, LOUIS F. LIBELO, JR., SENIOR MEMBER, IEEE, AND GUY E. PISANE

Abstract—**The generalized dual series solution to the scattering of an arbitrary plane wave from an open spherical shell having a circular aperture and enclosing a concentric homogeneous dielectric sphere is presented. This solution explicitly exhibits the correct edge behavior, and it can handle spheres that are electrically small or large without special considerations. A variety of cross section results is presented for the normally incident case. It is shown that effects corresponding to the presence of the interior cavity dominate all of the scattering data. In particular, the cross sections exhibit new resonance features that are due to the cavity-backed nature of the aperture and depend on the characteristics of the interior sphere. The results demonstrate that interior information is contained in the exterior scattering data.**

I. INTRODUCTION

BECAUSE they describe coupling via apertures into enclosed regions containing additional dielectric or metallic bodies *and* scattering from reflector structures having edges and nontrivial configurations, the importance of canonical electromagnetic cavity-backed aperture problems cannot be overstated. They provide a fundamental means with which basic aperture coupling and reflector physics can be studied in detail; they can be used to construct and/or validate approximate models or general engineering analysis and design "rules of thumb" that can be applied to more general apertures and scattering objects; and they aid in the development of improved numerical techniques especially near the edges of the apertures or reflectors where discontinuities appear and where those methods may encounter difficulties. Moreover, accurate canonical solutions of this type provide standards to which general-purpose numerical code results can be compared.

A number of canonical problems that describe coupling through apertures into enclosed regions have been solved recently with the generalized dual series (GDS) approach and have been reported elsewhere [1]–[5]. In two dimensions these include the scattering of E- and H-polarized plane waves from an empty infinite circular cylinder having an infinite axial slot [1], [2] and from one that encloses an infinite concentric [3], [4] or offset impedance cylinder [5]. These two-dimensional slit cylinder problems have proved valuable for nuclear electromagnetic pulse (EMP) studies. The locations of field hotspots near the interior object and the current peaks induced on an interior wire are being studied as a function of all of the problem parameters. In three dimensions the scattering of an arbitrary plane wave from an empty open spherical shell with a circular aperture has been solved [6], [7]. These problems have been studied extensively to determine the effects on the aperture coupling and scattering of variations in the polarization, frequency, angle of incidence, aperture size, and interior object characteristics. The GDS solutions are systematic and inherently contain the behavior near the rim of the aperture required by Meixner's edge conditions. They can handle open spheres that are electrically small or large and arbitrary angles of incidence without additional special considerations. The three-dimensional open spherical shell problems are important because they involve a finite scatterer for which experimental data can be obtained [8].

In this paper we extend the open spherical shell solution to the case where it encloses a concentric homogeneous dielectric sphere. Because of length considerations, we will discuss only the normally incident case. As will be described, these results are readily extended to an incidence angle as described in [6].

This dual series solution is the first of its kind for a loaded open-sphere problem. On the other hand, the closed spherical cavity loaded with a concentric lossy dielectric core has been analyzed for microwave fusion studies [9]–[12]. Initial heating rates of a plasma core and perturbations of the eigenmodes caused by deformations of the plasma core were investigated. The closed loaded cavity problem results were recently extended to aid in the explanation of the resonance phenomena to be presented [13].

It has been found that resonance features corresponding to the presence of the interior cavity dominate all of the aperture coupling and the scattering results. These include the currents induced on the exterior scatterer, the fields in the aperture, the energy captured by the open cavity, and the scattering cross sections. As will be demonstrated, the locations in frequency of these cavity-backed aperture (CBA) resonances and the resultant current and field patterns at those values can be identified with corresponding closed-cavity resonance locations and patterns.

Manuscript received February 6, 1987; revised November 25, 1987. This work was supported in part by the U.S. Department of Energy and the Lawrence Livermore National Laboratory under Contract W-7405-ENG-48 and in part by the Harry Diamond Laboratories.

R. W. Ziolkowski is with the Engineering Research Division, Lawrence Livermore National Laboratory, PO Box 5504, L-156, Livermore, CA 94550.

D. P. Marsland was with the Engineering Research Division, Lawrence Livermore National Laboratory, Livermore, CA. She is now with SRI International, Menlo Park, CA 94025.

L. F. Libelo, Jr., and G. E. Pisane are with the Harry Diamond Laboratories, 2800 Power Mill Road, Adelphi, MD 20783.

IEEE Log Number 8820227.

0018-926X/88/0700-0985$01.00

II. Description of the Problem

A cross section of the generic problem configuration is shown in Fig. 1. A perfectly conducting, infinitesimally thin, open spherical shell is represented by the surface $\{r = a, 0 \leq \theta < \theta_0\}$ in the spherical coordinate system (r, θ, ϕ) erected at the shell's center. The negative z axis of that system passes through the center of the aperture, the latter being defined as $\{(r, \theta, \phi) | r = a \text{ and } \theta_0 < \theta \leq \pi\}$. The interior dielectric sphere has a radius b and a dielectric constant $\epsilon = \epsilon_r \epsilon_0$, where ϵ_0 is the dielectric permittivity of free space. Half the angular extent of the aperture is measured by the angle $\theta_{ap} = \pi - \theta_0$. The unit vectors $(\hat{r}, \hat{\theta}, \hat{\phi})$ are defined in the standard manner in the directions of positively increasing coordinate values. We divide the problem space into three radial subregions defined as follows:

Region I: $\{(r, \theta, \phi) | r > a\}$
Region II: $\{(r, \theta, \phi) | b < r < a\}$
Region III: $\{(r, \theta, \phi) | r < b\}$.

A plane wave

$$\begin{pmatrix} \vec{E}^{\text{inc}} \\ \vec{H}^{\text{inc}} \end{pmatrix} (r, \theta, \phi) = -E_0 e^{i\vec{k}\cdot\vec{r}} \begin{pmatrix} \hat{x} \\ Y_0 \cos\theta^{\text{inc}} \hat{y} \end{pmatrix} \quad (1)$$

is normally incident on the open sphere. Throughout this paper, an $e^{-i\omega t}$ time dependence is assumed and suppressed. The incident angles $\theta^{\text{inc}} = 0$ or π; $\phi^{\text{inc}} = 0$.

Following standard analyses of problems in a spherically symmetric geometry, we employ a Debye potential formalism. In particular, if the radial vector $\vec{r} = r\hat{r}$, the electric and magnetic fields are expressed in terms of the two Hertzian potentials $\Phi\vec{r}$ and $\Psi\vec{r}$ as

$$\vec{E} = -\text{curl}\,(\Phi\vec{r}) - (i\omega\epsilon)^{-1}\,\text{curl curl}\,(\Psi\vec{r})$$

$$\vec{H} = +\text{curl}\,(\Psi\vec{r}) - (i\omega\mu)^{-1}\,\text{curl curl}\,(\Phi\vec{r}). \quad (2)$$

The function $\Phi = \sum_{m=0}^{\infty}\sum_{n=m}^{\infty}\Phi_{mn}\sin m\phi$ defines the field TE with respect to r, $\Psi = \sum_{m=0}^{\infty}\sum_{n=m}^{\infty}\Psi_{mn}\cos m\phi$ the field TM with respect to r. The assumption of normal incidence reduces these potentials to a single azimuthal mode for both the incident and the scattered fields:

$$\begin{pmatrix} \Phi^{\text{inc}} \\ \Phi^{s} \end{pmatrix} (r, \theta, \phi) = \sum_{n=1}^{\infty} \begin{pmatrix} \Phi_{1n}^{\text{inc}} \\ \Phi_{1n}^{s} \end{pmatrix} (r, \theta) \sin\phi$$

$$\begin{pmatrix} \Psi^{\text{inc}} \\ \Psi^{s} \end{pmatrix} (r, \theta, \phi) = \sum_{n=1}^{\infty} \begin{pmatrix} \Psi_{1n}^{\text{inc}} \\ \Psi_{1n}^{s} \end{pmatrix} (r, \theta) \cos\phi.$$

The actual form of the azimuthal modal coefficients of the scattered field, Φ_1^s and Ψ_1^s, depends upon in which region r lies. Enforcing the electromagnetic boundary conditions:

1) $E_{\text{tan}}^{\text{tot}}$, $H_{\text{tan}}^{\text{tot}}$ must be continuous across $r = b$,
2) $E_{\text{tan}}^{\text{tot}}$ must be continuous across $r = a$;

we obtain fields from (2) that are summarized by the

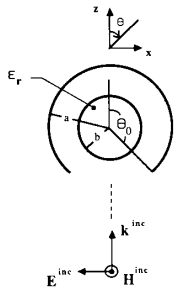

Fig. 1. Generic configuration of a scattering of a plane wave from a cavity-backed aperture with an interior dielectric load.

expressions:

$$E_r = E_0 \sum_{n=1}^{\infty} \left\{ in(n+1)\tau_{1n} \frac{Z_n(kr)}{kr} \bar{v}_{1n}(\theta) \right\} \sin\theta\cos\phi$$

$$E_\theta = E_0 \sum_{n=1}^{\infty} \left\{ \sigma_{1n} Z_n(kr) \bar{v}_{1n}(\theta) - i\tau_{1n} \frac{[krZ_n(kr)]'}{kr} \bar{w}_{1n}(\theta) \right\} \cos\phi$$

$$E_\phi = E_0 \sum_{n=1}^{\infty} \left\{ \sigma_{1n} Z_n(kr) \bar{w}_{1n}(\theta) - i\tau_{1n} \frac{[krZ_n(kr)]'}{kr} \bar{v}_{1n}(\theta) \right\} \sin\phi$$

$$H_r = -Y_0 E_0 \sum_{n=1}^{\infty} \left\{ in(n+1)\sigma_{1n} \frac{Z_n(kr)}{kr} \bar{v}_{1n}(\theta) \right\} \sin\theta\sin\phi$$

$$H_\theta = -Y_0 E_0 \sum_{n=1}^{\infty} \left\{ \tau_{1n} Z_n(kr) \bar{v}_{1n}(\theta) - i\sigma_{1n} \frac{[krZ_n(kr)]'}{kr} \bar{w}_{1n}(\theta) \right\} \sin\phi$$

$$H_\phi = -Y_0 E_0 \sum_{n=1}^{\infty} \left\{ \tau_{1n} Z_n(kr) \bar{w}_{1n}(\theta) - i\sigma_{1n} \frac{[krZ_n(kr)]'}{kr} \bar{v}_{1n}(\theta) \right\} \cos\phi, \quad (3)$$

where the terms $\bar{v}_{mn}(\theta) = mP_n^{-m}(\cos\theta)/\sin\theta$ and $\bar{w}_{mn}(\theta) = -\partial_\theta P_n^{-m}(\cos\theta)$, and the notation, for example, $[xj_n(x)]'$, means to take the derivative of the expression in the brackets with respect to x. The function $Z_n(kr)$ is composed of linear combinations of spherical Bessel, $j_n(kr)$; Neumann, $n_n(kr)$; and Hankel (of the first kind), $h_n(kr)$ functions depending on the value of r. In particular, for the *incident field* one has for any r: $Z_n(kr) = j_n(kr)$ and the coefficients

$$\begin{pmatrix} \sigma_{mn}^{\text{inc}} \\ \tau_{mn}^{\text{inc}} \end{pmatrix} = (-1)^{m+1} i^n \frac{(2n+1)}{n(n+1)} \epsilon_m (1 - \delta_{0n}) \begin{pmatrix} \bar{v}_{1n} \\ \bar{w}_{1n} \end{pmatrix} (\theta = \theta^{\text{inc}})$$

where $\epsilon_m = 1$ if $m = 0$ and $=2$ if $m \neq 0$ and Kronecker's delta $\delta_{0n} = 1$ if $n = 0$ and $=0$ if $n \neq 0$. For *normal incidence* these coefficients explicitly reduce to the values:

$$\begin{pmatrix} \sigma_{1n}^{\text{inc}} \\ \tau_{1n}^{\text{inc}} \end{pmatrix} (\theta^{\text{inc}} = 0) = i^n (2n+1) \begin{pmatrix} +1 \\ -1 \end{pmatrix}$$

$$\begin{pmatrix} \sigma_{1n}^{\text{inc}} \\ \tau_{1n}^{\text{inc}} \end{pmatrix} (\theta^{\text{inc}} = \pi) = -(-i)^n (2n+1) \begin{pmatrix} +1 \\ +1 \end{pmatrix}. \quad (4)$$

With the notation

$$\eta_n^e = \frac{j_n(kb)[k'bj_n(k'b)]' - j_n(k'b)[kbj_n(kb)]'}{j_n(k'b)[kbh_n(kb)]' - h_n(kb)[k'bj_n(k'b)]'}$$

$$\eta_n^h = \frac{j_n(kb)[k'bj_n(k'b)]' - \epsilon_r j_n(k'b)[kbj_n(kb)]'}{\epsilon_r j_n(k'b)[kbh_n(kb)]' - h_n(kb)[k'bj_n(k'b)]'} \quad (5a)$$

$$\xi_n^e(kr) = j_n(kr) + \eta_n^e h_n(kr)$$

$$\xi_n^h(kr) = j_n(kr) + \eta_n^h h_n(kr) \quad (5b)$$

$$\zeta_n^e(k'r) = \left(\frac{i}{kb}\right) \cdot \frac{j_n(k'r)}{j_n(k'b)[kbh_n(kb)]' - h_n(kb)[k'bj_n(k'b)]'}$$

$$\zeta_n^h(k'r) = \left(\frac{i}{kb}\right) \cdot \frac{\epsilon_r j_n(k'r)}{\epsilon_r j_n(k'b)[kbh_n(kb)]' - h_n(kb)[k'bj_n(k'b)]'}, \quad (5c)$$

the total field expressions then have the form

$$\begin{pmatrix} \sigma_{1n} \\ \tau_{1n} \end{pmatrix} Z_n(kr) = \begin{pmatrix} A_{1n}\xi_n^e(ka) \\ B_{1n}[ka\xi_n^h(ka)]' \end{pmatrix} h_n(kr) + \begin{pmatrix} \sigma_{1n}^{\text{inc}}\xi_n^e(kr) \\ \tau_{1n}^{\text{inc}}\xi_n^h(kr) \end{pmatrix} \quad \text{in Region I} \quad (6a)$$

$$\begin{pmatrix} \sigma_{1n} \\ \tau_{1n} \end{pmatrix} Z_n(kr) = \begin{pmatrix} [A_{1n}h_n(ka) + \sigma_{1n}^{\text{inc}}]\xi_n^e(kr) \\ \{B_{1n}[kah_n(ka)]' + \tau_{1n}^{\text{inc}}\}\xi_n^h(kr) \end{pmatrix} \quad \text{in Region II} \quad (6b)$$

$$\begin{pmatrix} \sigma_{1n} \\ \tau_{1n} \end{pmatrix} Z_n(k'r) = \begin{pmatrix} [A_{1n}h_n(ka) + \sigma_{1n}^{\text{inc}}]\zeta_n^e(k'r) \\ \{B_{1n}[kah_n(ka)]' + \tau_{1n}^{\text{inc}}\}\zeta_n^h(k'r) \end{pmatrix} \quad \text{in Region III.} \quad (6c)$$

It is readily verified by inspection that the resulting electric fields are continuous across $r = a$ and because $\xi_n^{e,h}(kb) = \zeta_n^{e,h}(kb)$, the electric and magnetic fields are continuous across $r = b$. We now proceed as in [6].

The dual series equations are obtained by enforcing the electromagnetic boundary equations: $E_{\tan}^{\text{tot}} = 0$ on the open metallic shell and $H_{\tan}^{\text{tot}}$ is continuous over the circular aperture. With the field expressions (5) and the terms

$$f_{1n} = \sigma_{1n}^{\text{inc}}\xi_n^e(ka)$$

$$g_{1n} = \tau_{1n}^{\text{inc}}\xi_n^h(ka), \quad (7)$$

one obtains

$$ika \sum_{n=1}^{\infty} \{A_{1n}\xi_n^e(ka)h_n(ka) - f_{1n}\} P_n^{-1} = \sin\theta\partial_\theta \sum_{n=1}^{\infty} \{B_{1n}[ka\xi_n^h(ka)]'[kah_n(ka)]' - g_{1n}\} P_n^{-1}, \quad 0 \leq \theta < \theta_0 \quad (8a)$$

$$\sum_{n=1}^{\infty} A_{1n}P_n^{-1} = -ika \sin\theta\partial_\theta \sum_{n=1}^{\infty} B_{1n}P_n^{-1}, \quad \theta_0 < \theta \leq \pi \quad (8b)$$

$$ika \sin\theta\partial_\theta \sum_{n=1}^{\infty} \{A_{1n}\xi_n^e(ka)h_n(ka) - f_{1n}\} P_n^{-1} = \sum_{n=1}^{\infty} \{B_{1n}[ka\xi_n^h(ka)]'[kah_n(ka)]' - g_{1n}\} P_n^{-1}, \quad 0 \leq \theta < \theta_0 \quad (9a)$$

$$\sin\theta\partial_\theta \sum_{n=1}^{\infty} A_{1n}P_n^{-1} = -ika \sum_{n=1}^{\infty} B_{1n}P_n^{-1}, \quad \theta_0 < \theta \leq \pi. \quad (9b)$$

These coupled dual series equations differ from those obtained in [6] only through the presence of the terms proportional to η_n^e and η_n^h. Those terms have the same large n behavior as the "original" ones in [6]. In particular, we can define the functions

$$\chi_n^\phi = [ika(2n+1)\xi_n^e(ka)h_n(ka)] - 1 \quad (10a)$$

$$\bar{\chi}_n^\psi = -\left\{1 + \frac{4ika}{2n+1}[ka\xi_n^h(ka)]'[kah_n(ka)]'\right\} \quad (10b)$$

which, as n becomes large, behave as $\lim_{n\to\infty} \chi_n^\circ \sim O(n^{-2})$ and $\lim_{n\to\infty} \bar{\chi}_n^\psi \sim O(n^{-2})$. Consequently, we can use the normal incidence results of [6] immediately to obtain a coupled system of infinite linear equations for the unknown modal coefficients. With the truncation procedure introduced in [6], this system is reduced to a finite numerically tractable one of the form

$$(-2ikaL_{1l}^e)\bar{\beta}_1 + \frac{A_{1l}}{l+1/2} + \sum_{n=1}^{N} (\chi_n^\phi \Gamma_{1,nl}^e) \cdot \frac{A_{1n}}{n+1/2} = 2ika \sum_{n=1}^{N} \Gamma_{1,nl}^e f_{1n} \quad (11a)$$

$$(-L^h_{1l})\bar{\beta}_1 + B_{1l} + \sum_{n=1}^{N} (\tilde{\chi}^{\psi}_n \Gamma^h_{1,nl}) B_{1n}$$

$$= -2ika \sum_{n=1}^{N} \Gamma^h_{1,nl} \frac{g_{1n}}{n+1/2} \quad (11b)$$

$$[-2ika(1-\Lambda^e_{00})]\bar{\beta}_1 + (-2ika\Lambda^e_{00})\alpha_1 + \sum_{n=1}^{N} (\chi^{\phi}_n \Lambda^e_{n0}) \frac{A_{1n}}{n+1/2} = 2ika \sum_{n=1}^{N} \Lambda^e_{n0} f_{1n} \quad (11c)$$

$$[-(1-\Lambda^h_{00})]\bar{\beta}_1 + [-4(ka)^2\Lambda^h_{00}]\alpha_1 + \sum_{n=1}^{N} (\tilde{\chi}^{\psi}_n \Lambda^h_{n0}) B_{1n}$$

$$= -2ika \sum_{n=1}^{N} \Lambda^h_{n0} \frac{g_{1n}}{n+1/2}, \quad (11d)$$

where the inversion coefficients are

$$\Lambda^e_{nl} = \frac{1}{\pi}\left[\frac{\sin(n-l)\theta_0}{n-l} + \frac{\sin(n+l+1)\theta_0}{n+l+1}\right] \quad (12a)$$

$$\Lambda^h_{nl} = \frac{1}{\pi}\left[\frac{\sin(n-l)\theta_0}{n-l} - \frac{\sin(n+l+1)\theta_0}{n+l+1}\right] \quad (12b)$$

so that

$$\Gamma^{e,h}_{1,nl} = \frac{\Lambda^{e,h}_{nl}\Lambda^{e,h}_{00} - \Lambda^{e,h}_{n0}\Lambda^{e,h}_{0l}}{\Lambda^{e,h}_{00}} \quad (12c)$$

$$L^{e,h}_{1l} = -\frac{\Lambda^{e,h}_{0l}}{\Lambda^{e,h}_{00}}. \quad (12d)$$

The constants α_1 and $\bar{\beta}_1$ are introduced in the solution process to permit a pseudo-decoupling [6], [14] of the TE and the TM dual series equations systems and to guarantee satisfaction of Meixner's edge conditions. This system can be solved for the modal coefficients A_{1l} and B_{1l} with $l = 1, 2, \cdots, N$, for instance, by Gauss elimination. Any additional coefficients up to some value L can then be generated recursively from (11) by setting $l = N+1, N+2, \cdots, L$. Brute force summations of the resulting modal series that represent quantities such as the field components transverse or the current components parallel to the edge of the aperture, which inherently contain (square root) singularities, exhibit Gibbs' phenomena and require these additional coefficients to realize convergence [6]. However, these difficulties can be circumvented through the use of the analytical preconditioning procedure developed in [6]. Introducing the asymptotic large index behavior of the solution coefficients, one can extract sums that can be handled analytically. The remaining sums converge rapidly numerically, thus eliminating the need for these additional coefficients. Convergence of the desired solution coefficients and of the subsequent series representing various electromagnetic quantities is obtained typically with a value of $N = 10ka$ so that $(ka/N)^2$ is small. The following results are derived from (11) in this manner. The desired modal coefficients for open loaded spheres that are electrically small or large are thus generated with this GDS approach simply by choosing the appropriate value of N without any further considerations.

In the quasi-static limit analytical expressions can be derived that readily recover the results given, for instance, by Casey in [15] for field penetration into an unloaded spherical cavity and their extensions to the corresponding loaded cavity cases. When the aperture is small, approximate expressions can also be obtained. These would provide an interesting check on perturbational analyses of this configuration. Nonnormal incidence cases are treated in a similar fashion by solving systems analogous to (11) for each azimuthal mode and then incorporating the requisite azimuthal mode sums in the desired observables. The associated inversion coefficients analogous to $\Gamma^{e,h}_{1,nl}$ and $L^{e,h}_{1l}$ are derived in [6].

III. Results

Any electromagnetic quantity can be calculated once the modal coefficients are determined. In our analysis of the coupling of the plane wave to the dielectrically loaded open sphere, we have stressed the scattering cross sections (bistatic, radar, forward, and total differential) of this system and the total energy captured by it. The associated formulas for these quantities will be given below before the discussion of the numerical results.

A. Requisite Formulas

The scattering cross sections all deal with the far-field behavior of the scattered fields. In particular, the bistatic cross section is given by the expression:

$$\sigma_{BS}(\theta, \phi; \theta^{inc}, \phi^{inc}) = \lim_{r\to\infty} 4\pi r^2 \frac{|E^s(r,\theta,\phi)|^2}{|E^{inc}(r,\theta,\phi)|^2}$$

$$= \frac{4\pi}{k^2}\left\{\left|\sum_{n=1}^{\infty}(-1)^n[\sigma^I_{1n}\bar{v}_{1n}(\theta) + \tau^I_{1n}\bar{w}_{1n}(\theta)]\right|^2 \cos^2\phi + \left|\sum_{n=1}^{\infty}(-1)^n[\sigma^I_{1n}\bar{w}_{1n}(\theta) + \tau^I_{1n}\bar{v}_{1n}(\theta)]\right|^2 \sin^2\phi\right\} \quad (13)$$

which for $\theta = \theta^{inc} + \pi$ and $\phi = \phi^{inc}$ gives the radar cross section:

$$\sigma_{RCS} = \sigma_{BS}(\theta^{inc}+\pi, \phi^{inc}; \theta^{inc}, \phi^{inc}) = \frac{\pi}{k^2}\left|\sum_{n=-\infty}^{\infty} i^n[\sigma^I_{1n} + \tau^I_{1n}]\right|^2 \quad (14)$$

which for $\theta = \theta^{inc}$ and $\phi = \phi^{inc}$ gives the forward cross section:

$$\sigma_{FCS} = \sigma_{BS}(\theta^{inc}, \phi^{inc}; \theta^{inc}, \phi^{inc}) = \frac{\pi}{k^2}\left|\sum_{n=-\infty}^{\infty}(-i)^n[\sigma^I_{1n} - \tau^I_{1n}]\right|^2, \quad (15)$$

where from (6a) the scattered field coefficients for $r > a$ are defined as

$$\sigma_{1n}^{I} = A_{1n}\xi_n^e(ka) + \eta_n^e \sigma_{1n}^{\text{inc}} \tag{16a}$$

$$\tau_{1n}^{I} = B_{1n}[ka\xi_n^h(ka)]' + \eta_n^h \tau_{1n}^{\text{inc}}. \tag{16b}$$

These cross sections indicate the amount of field scattered in particular directions. To make a connection of these formulas with the standard ones for the closed sphere, notice that in the limit $\theta_0 \to \pi$, where the shell is closed, the empty sphere solution coefficients reduce to the forms [6]

$$A_{1n}(\theta_0 = \pi) = -\frac{i^n(2n+1)}{h_n(ka)} = (2n+1)\frac{a_n}{j_n(ka)}$$

$$B_{1n}(\theta_0 = \pi) = \frac{i^n(2n+1)}{[kah_n(ka)]'} = -(2n+1)\frac{b_n}{[kaj_n(ka)]'}.$$

Consequently, the standard closed sphere radar cross section result is, for instance, recovered:

$$\sigma_{\text{RCS}}^{\text{closed}} = \frac{\pi}{k^2}\left|\sum_{n=1}^{\infty}(-1)^{n+1}(2n+1)(a_n - b_n)\right|^2. \tag{17}$$

In contrast, the total differential or scattering cross section

$$\sigma_{\text{tot}} = \lim_{r\to\infty}\frac{\frac{1}{2}\int \text{Re}\,[(\vec{E}_s \times \vec{H}_s^*)\cdot \hat{r}]r^2 \sin\theta\, d\theta d\phi}{\frac{1}{2}Y_0|E_0|^2}$$

$$= \frac{2\pi}{k^2}\sum_{n=1}^{\infty}\frac{[|\sigma_{1n}^{I}|^2 + |\tau_{1n}^{I}|^2]}{2n+1} \tag{18}$$

is representative of the energy scattered into the entire 4π-sphere.

The total energy captured by the open scattering object is an important measure of the amount of coupling the incident field experiences through the aperture into the object's interior. The total energy captured in the dielectrically loaded open sphere is given by the complicated expression

$$U_{\text{tot}} = \frac{1}{2}\int_0^b\int_0^{\pi}\int_0^{2\pi}[|\vec{E}^{\text{III}}|^2 + |Z_0\vec{H}^{\text{III}}|^2]r^2\sin\theta\, dr\, d\theta\, d\phi$$

$$+\frac{1}{2}\int_b^a\int_0^{\pi}\int_0^{2\pi}[|\vec{E}^{\text{II}}|^2 + |Z_0\vec{H}^{\text{II}}|^2]r^2\sin\theta\, dr\, d\theta\, d\phi$$

$$= 2\pi E_0^2 b^3\sum_{n=1}^{\infty}(2n+1)|u_n^{\text{III}}|^2$$

$$\cdot [j_n^2(k'b) - j_{n-1}(k'b)j_{n+1}(k'b)]$$

$$+2\pi E_0^2\sum_{n=1}^{\infty}(2n+1)\left\{|u_{1n}^{\text{II}}|^2\right.$$

$$\cdot \{a^3[j_n^2(ka) - j_{n-1}(ka)j_{n+1}(ka)]$$

$$-b^3[j_n^2(kb) - j_{n-1}(kb)j_{n+1}(kb)]\}$$

$$+|u_{2n}^{\text{II}}|^2\left\{a^3[j_n(ka)n_n(ka)\right.$$

$$-\frac{1}{2}\{j_{n+1}(ka)n_{n-1}(ka) + j_{n-1}(ka)n_{n+1}(ka)\}]$$

$$-b^3[j_n(kb)n_n(kb) - \frac{1}{2}\{j_{n+1}(kb)n_{n-1}(kb)$$

$$\left.+j_{n-1}(kb)n_{n+1}(kb)\}]\right\}$$

$$\left.+|u_{3n}^{\text{II}}|^2\{a^3[n_n^2(ka) - n_{n-1}(ka)n_{n+1}(ka)]\right.$$

$$\left.-b^3[n_n^2(kb) - n_{n-1}(kb)n_{n+1}(kb)]\}\right] \tag{19}$$

where the following notation has been introduced:

$$|u_n^{\text{III}}|^2 = \frac{|\sigma_{1n}^{\text{III}}|^2 + |\tau_{1n}^{\text{III}}|^2}{(2n+1)^2} \tag{20a}$$

$$|u_{1n}^{\text{II}}|^2 = \frac{|\sigma_{1n}^{\text{II}}|^2(1 + 2\eta_n^{e,r} + |\eta_n^e|^2) + |\tau_{1n}^{\text{II}}|^2(1 + 2\eta_n^{h,r} + |\eta_n^h|^2)}{(2n+1)^2} \tag{20b}$$

$$|u_{2n}^{\text{II}}|^2 = \frac{|\sigma_{1n}^{\text{II}}|^2(2\eta_n^{e,i}) + |\tau_{1n}^{\text{II}}|^2(2\eta_n^{h,i})}{(2n+1)^2} \tag{20c}$$

$$|u_{3n}^{\text{II}}|^2 = \frac{|\sigma_{1n}^{\text{II}}|^2|\eta_n^e|^2 + |\tau_{1n}^{\text{II}}|^2|\eta_n^h|^2}{(2n+1)^2} \tag{20d}$$

where, for instance, $\eta_n^{e,r}$ is the real part of η_n^e, and from (6b) and (6c) the coefficients

$$\sigma_{1n}^{\text{II}} = A_{1n}h_n(ka) + \sigma_{1n}^{\text{inc}} \tag{21a}$$

$$\tau_{1n}^{\text{II}} = B_{1n}[kah_n(ka)]' + \tau_{1n}^{\text{inc}} \tag{21b}$$

$$\sigma_{1n}^{\text{III}} = \frac{i}{kb}\frac{A_{1n}h_n(ka) + \sigma_{1n}^{\text{inc}}}{j_n(k'b)[kbh_n(kb)]' - h_n(kb)[k'bj_n(k'b)]'} \tag{21c}$$

$$\tau_{1n}^{\text{III}} = \frac{i}{kb}\frac{\epsilon_r\{B_{1n}[kah_n(ka)]' + \tau_{1n}^{\text{inc}}\}}{\epsilon_r j_n(k'b)[kbh_n(kb)]' - h_n(kb)[k'bj_n(k'b)]'}. \tag{21d}$$

The results for the total energy will be presented as a figure of merit defined by the ratio: $U_{\text{tot}}/U_{\text{inc}}$, of the total field energy in the dielectrically loaded open sphere to the incident field energy in the corresponding dielectrically loaded mathematical sphere with $r \leq a$:

$$U_{\text{inc}} = 2\pi E_0^2\sum_{n=1}^{\infty}(2n+1)|u_n^{\text{inc}}|^2$$

$$\cdot \{b^3[j_n^2(k'b) - j_{n-1}(k'b)j_{n+1}(k'b)]$$

$$+a^3[j_n^2(ka) - j_{n-1}(ka)j_{n+1}(ka)]$$

$$-b^3[j_n^2(kb) - j_{n-1}(kb)j_{n+1}(kb)]\} \tag{22a}$$

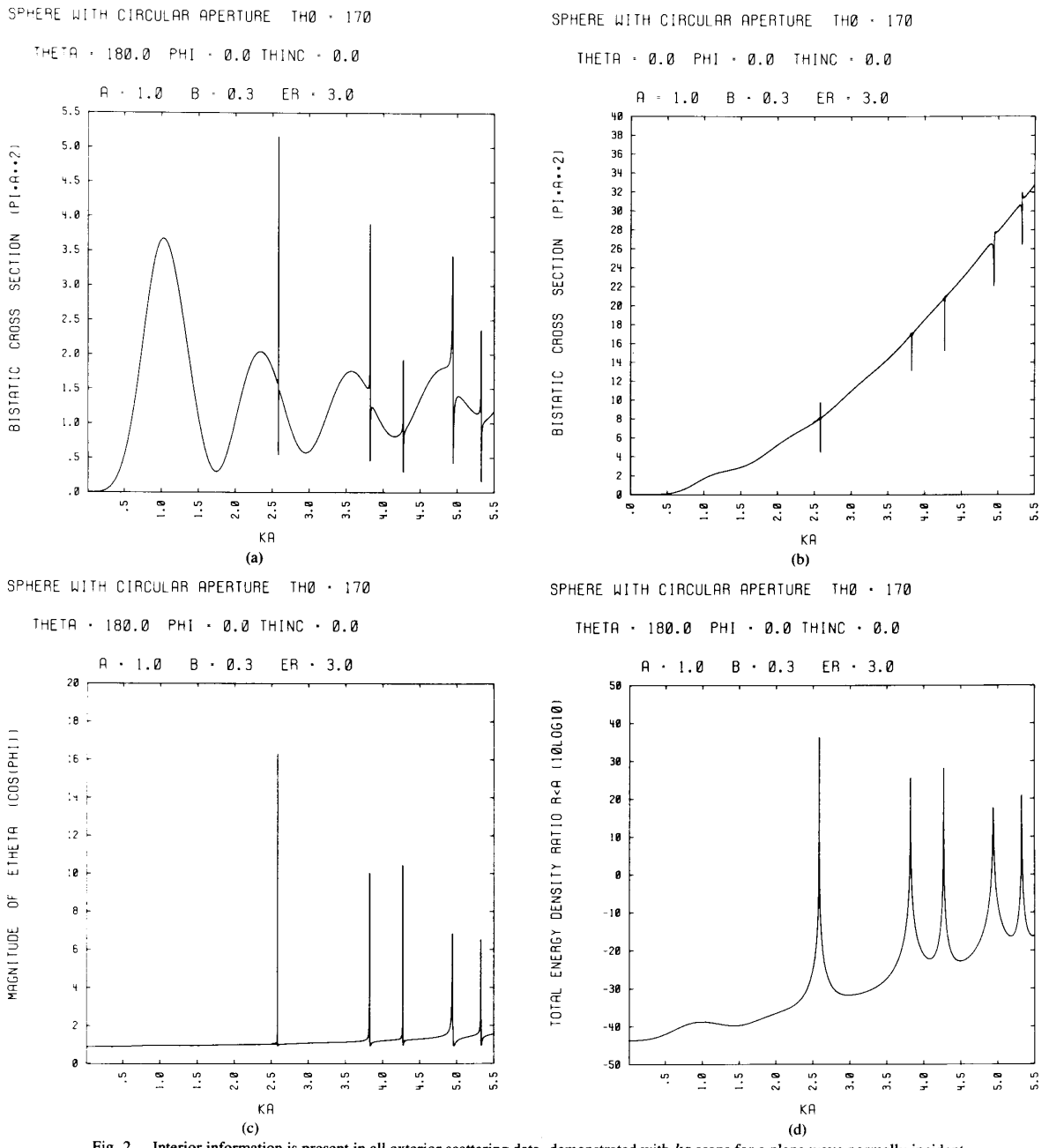

Fig. 2. Interior information is present in all exterior scattering data, demonstrated with ka scans for a plane wave normally incident into a 10° aperture of an open spherical shell of radius a enclosing a concentric dielectric of radius $b = 0.3a$ and relative permittivity $\epsilon_r = 3.0$. (a) Radar cross section. (b) Forward cross section. (c) Magnitude of E_θ at center of aperture. (d) Energy density ratio $U_{\text{tot}}/U_{\text{inc}}$.

where the coefficients

$$|u_n^{\text{inc}}|^2 = \frac{|\sigma_{1n}^{\text{inc}}|^2 + |\tau_{1n}^{\text{inc}}|^2}{(2n+1)^2}. \tag{22b}$$

B. Numerical Results

The dominance of the resonance features, corresponding to the presence of the interior cavity, in all of the aperture coupling and scattering results is first illustrated in Fig. 2. Included are the radar (Fig. 2(a)) and forward (Fig. 2(b)) cross sections normalized to πa^2, the aperture field $E_\theta^s(a, \pi, 0)$ (Fig. 2(c)), and the energy density ratio $U_{\text{tot}}/U_{\text{inc}}$ (Fig. 2(d)) for a unit amplitude plane wave incident at $\theta = 0°$ upon an open sphere with $\theta_{ap} = 10°$ and radius a enclosing a dielectric sphere of radius $b = 0.3a$ and relative permittivity $\epsilon_r = 3.0$. The peaks of the antiresonance features in the radar cross

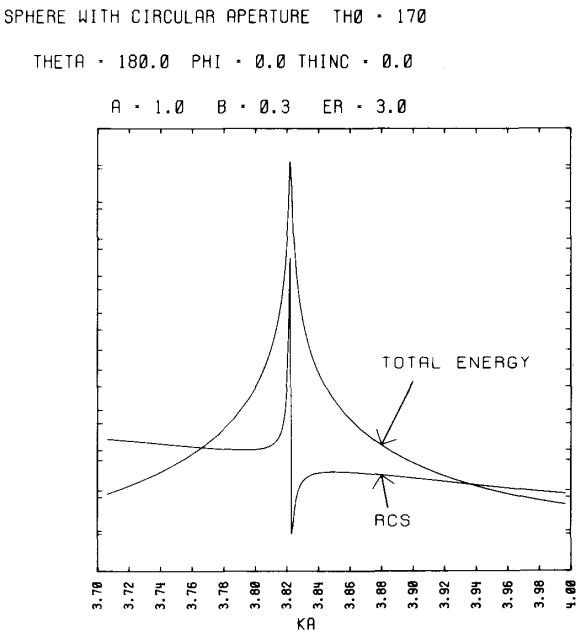

Fig. 3. Superimposed enhanced rendering of TM_{21} resonance regions of Fig. 2(a) and (d) elucidating reradiation behavior of cavity-backed aperture system.

section occur at ka = 2.5825, 3.822, 4.271, 4.939, and 5.326, and correspond to the TM_{11}, TM_{21}, TE_{11}, TM_{31}, and TM_{12} modes. The corresponding valleys occur at ka = 2.5827, 3.823, 4.272, 4.945, and 5.328. These mode assignments were made by tracking the resonance locations from the corresponding closed sphere to the present open sphere cases [13].

As discussed in [16], the open-sphere results are closely correlated with the closed-sphere results at lower ka values except for the presence of the CBA resonance features. As ka increases (wavelength decreases) so that the incident wave can begin to sense the presence of the aperture and the interior cavity, the deviation of the open-sphere from the closed-sphere results increases. This effect is clearly perceived in Fig. 2(c) where for the closed sphere case the scattered field would have a unit amplitude at $(a, \pi, 0)$. The peaks in the resonance locations in Fig. 2(d) occur at ka = 2.5825, 3.822, 4.271, 4.942, and 5.327. These are slightly lower in ka than the corresponding closed cavity values: 2.5854, 3.833, 4.275, 4.966, and 5.332. This effect is due to the detuning of the cavity by the aperture.

The difference in locations of the peaks of σ_{RCS} and U_{tot}/U_{inc} is characteristic of a CBA configuration. In particular, consider Fig. 3 where the TM_{21} resonance region of Figs. 2(a) and (d) are superimposed. As discussed in [16], the resonance peaks are indicative of a reradiation phenomenon that is associated with the cavity-backed nature of the aperture. As indicated by Fig. 3, the energy contained within the open spherical shell dramatically increases at a CBA resonance. Concurrently, the currents induced on the sphere and (as a consequence) the scattered fields experience a π-phase shift as ka passes through one of these CBA resonances. Thus a scattered field, whose amplitude is enhanced by the energy resonantly captured in the cavity, is created that at different look angles either constructively or destructively interferes with the incident field. As the cavity begins to capture more energy, the radar return increases; while just after resonance the radar return is dramatically smaller and the captured energy begins to decrease. The radar returns then approach their closed-sphere values as the stored energy decreases further. This results in the distinctive antiresonance features present in the radar cross section.

These resonance features are also found in the bistatic cross sections at the same relative positions for all look angles. This is demonstrated in Fig. 4 where the E-plane bistatic cross section of the case in Fig. 2 is given for the look-angles θ = 180°, 135°, 90°, and 45° as functions of ka. As one might expect, the shapes and sizes of the cross sections as well as the individual resonance peaks vary with the angle of incidence and the bistatic look angles. This behavior is further evidenced in Fig. 5 where the E-plane bistatic cross sections is given as a function of the bistatic angle θ for ka = 3.8170 (Fig. 5(a)), 3.8220 (Fig. 5(b)), 3.8230 (Fig. 5(c)), and 3.8280 (Fig. 5(d)). Fig. 5(b) and (c) correspond, respectively, to the locations very near the peak and the minimum of the associated CBA antiresonance feature present in Fig. 2(a). Comparing Fig. 5(a)–(d) one finds that the enhanced response in the backscattered direction just before the peak of the resonance occurs at the expense of the signals scattered into the other look angles, particularly in the broadside direction. Similarly, the broadside response is enhanced at the expense of the backscattered signal just past the antiresonance minimum.

The fact that the resonance features are very narrow in Fig. 2 is indicative of the extremely high Q nature of the cavity. Increasing the aperture size broadens them, and their locations are translated to lower ka values corresponding to an increased detuning of the cavity. This is illustrated in Fig. 6 where the total differential cross sections for a unit amplitude plane wave with θ^{inc} = 0° is incident on open spheres of radius a with aperture angles θ_{ap} = 10° (Fig. 6(a)), 15° (Fig. 6(b)), 20° (Fig. 6(c)), and 30° (Fig. 6(d)), enclosing a dielectric sphere of radius $b = 0.3a$ and relative permittivity ϵ_r = 3.0. The corresponding radar cross sections are given in Fig. 7(a)–(d). The movement of the RCS peaks and valleys are readily traced as the aperture size increases.

The locations of the CBA resonances are also dependent on the characteristics of the interior load. This is demonstrated in Figs. 8 and 9. In Fig. 8 a unit amplitude plane wave with θ^{inc} = 0° is incident on open spheres each with radius a and an aperture angle θ_{ap} = 10° and enclosing dielectric spheres of relative permittivity ϵ_r = 3.0 and radii $b = 0.1a$ (Fig. 8(a)), $b = 0.3a$ (Fig. 8(b)), $b = 0.5a$ (Fig. 8(c)), $b = 0.8a$ (Fig. 8(d)). In Fig. 9 a unit amplitude plane wave with θ^{inc} = 0° is incident on open spheres each with a radius a and an aperture angle θ_{ap} = 10° and enclosing dielectric spheres of radii $b = 0.3a$ and relative permittivities ϵ_r = 1.0 (Fig. 9(a)), ϵ_r = 3.0 (Fig. 9(b)), and ϵ_r = 10.0 (Fig. 9(c)).

As observed in Figs. 8 and 9, there are clear distinctions between all of the cases depending on the properties of the

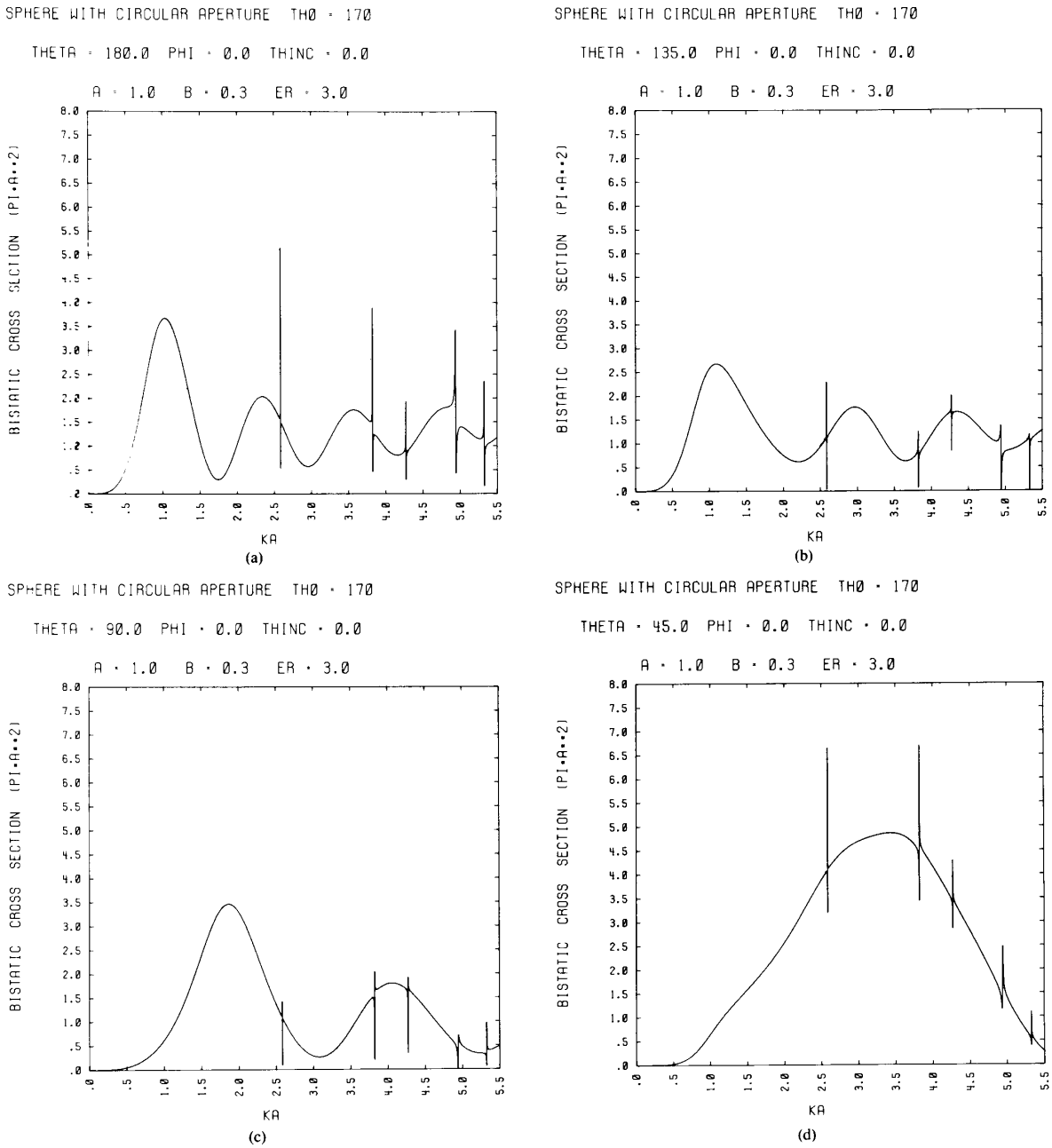

Fig. 4. CBA resonances are present at all bistatic look-angles, illustrated with E-plane bistatic cross section as function of ka for plane wave normally incident into a 10° aperture of an open spherical shell of radius a enclosing a concentric $\epsilon_r = 3.0$ dielectric sphere of radius $b = 0.3a$. (a) Observation angle $\theta = 180.0°$. (b) $\theta = 135.0°$. (c) $\theta = 90.0°$. (d) $\theta = 45.0°$.

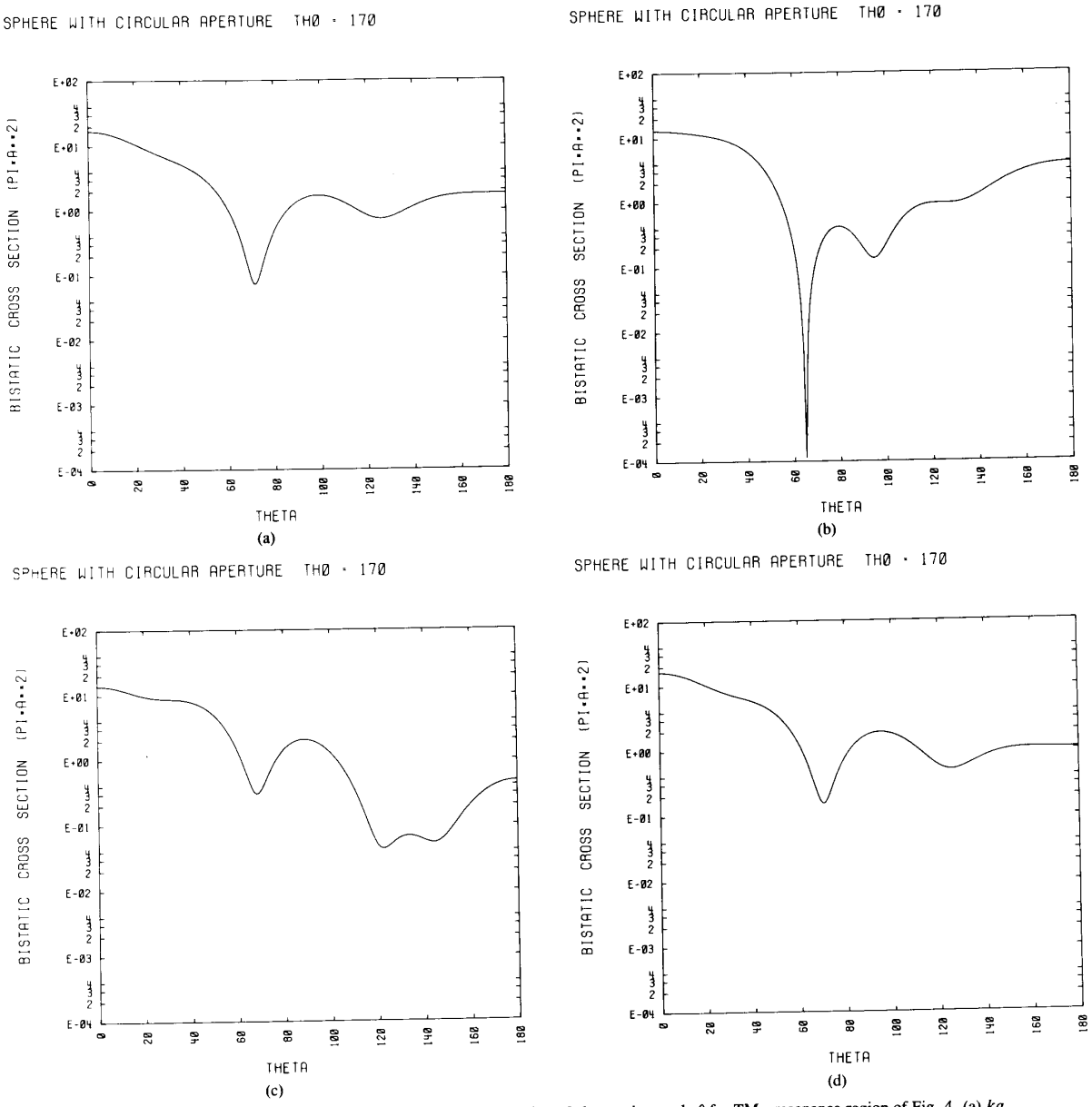

Fig. 5. More complete views of bistatic cross section as function of observation angle θ for TM_{21} resonance region of Fig. 4. (a) $ka = 3.8170$. (b) $ka = 3.8220$. (c) $ka = 3.8230$. (d) $ka = 3.8280$.

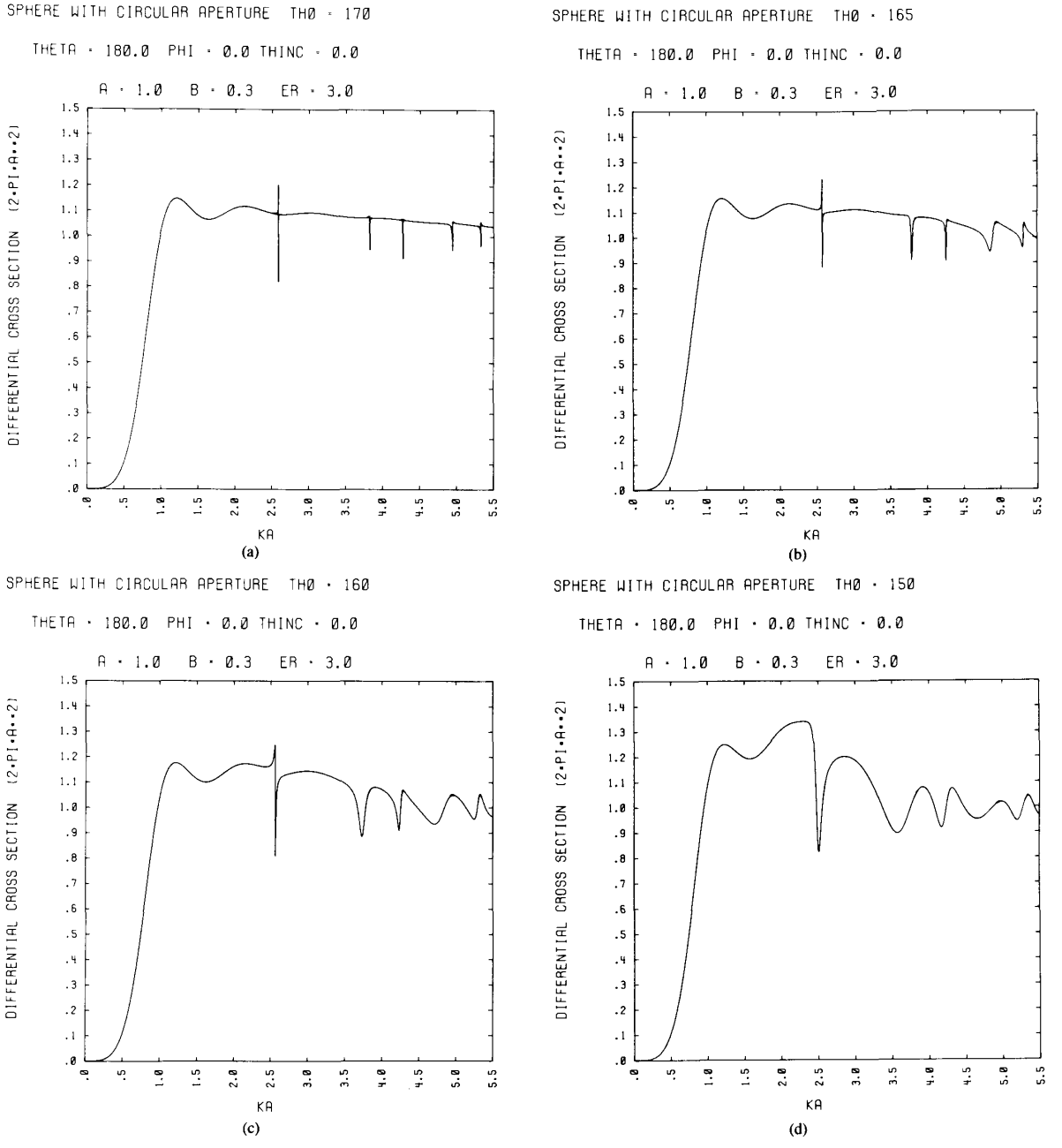

Fig. 6. As aperture size increases, cavity becomes more detuned and resonance features broaden and shift to lower ka, illustrated with total differential cross sections for a plane wave normally incident into open spherical shells of radius a with different apertures and enclosing a concentric $\epsilon_r = 3.0$ dielectric sphere of radius $b = 0.3a$. (a) Aperture = 10°. (b) 15°. (c) 20°. (d) 30°.

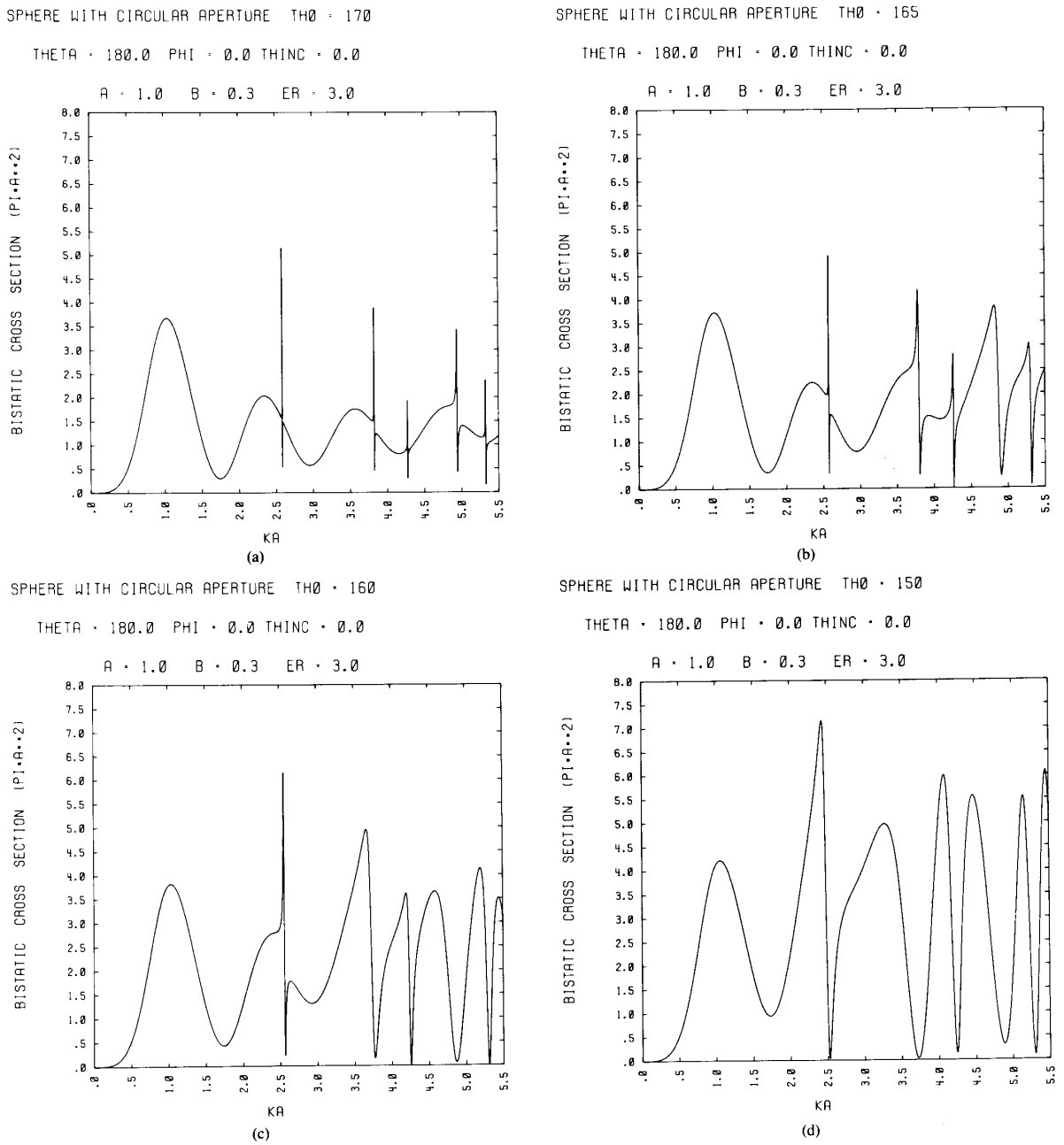

Fig. 7. Dual series solution allows one to track movement of CBA resonances as aperture size increases, illustrated with radar cross sections for plane wave normally incident into open spherical shells of radius a with different apertures and enclosing concentric $\epsilon_r = 3.0$ dielectric spheres of radius $b = 0.3a$. (a) Aperture = 10°. (b) 15°. (c) 20°. (d) 30°.

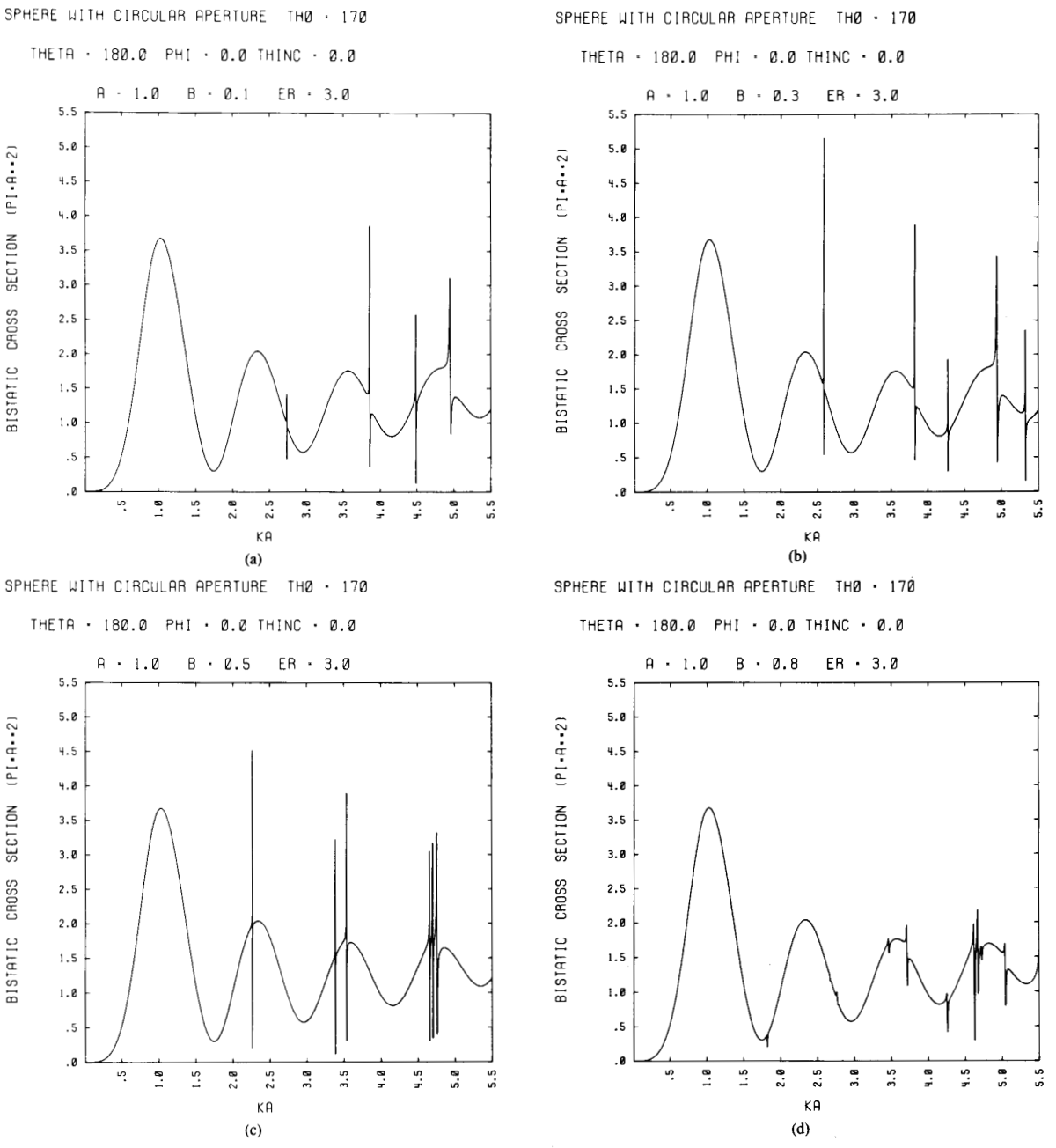

Fig. 8. Interior information contained in exterior scattering data, shown with radar cross sections for a plane wave normally incident into open spherical shells of radius a with a 10°, aperture and enclosing concentric $\epsilon_r = 3.0$ dielectric spheres. (a) Radius $b = 0.1a$. (b) $b = 0.3a$. (c) $b = 0.5a$. (d) $b = 0.8a$.

interior dielectric sphere. Some of the resonance locations are nearly coincident while others are not. This depends intimately on the particular modal pattern that is established in the interior of the cavity. If the mode "interacts" with the interior object, large shifts in the positions of the resonance features may be produced. Comparing the empty and the loaded cavity cases, one finds that as the size of the interior load is increased, very large translations of particular CBA resonance locations occur. As shown, one may observe the sequence in which resonances appear to be altered or even a disappearance of some or the apperance of additional resonances in a fixed ka interval. As the relative permittivity of the interior dielectric sphere is increased, the number of resonances found at lower ka values is dramatically increased. Of course, the number of

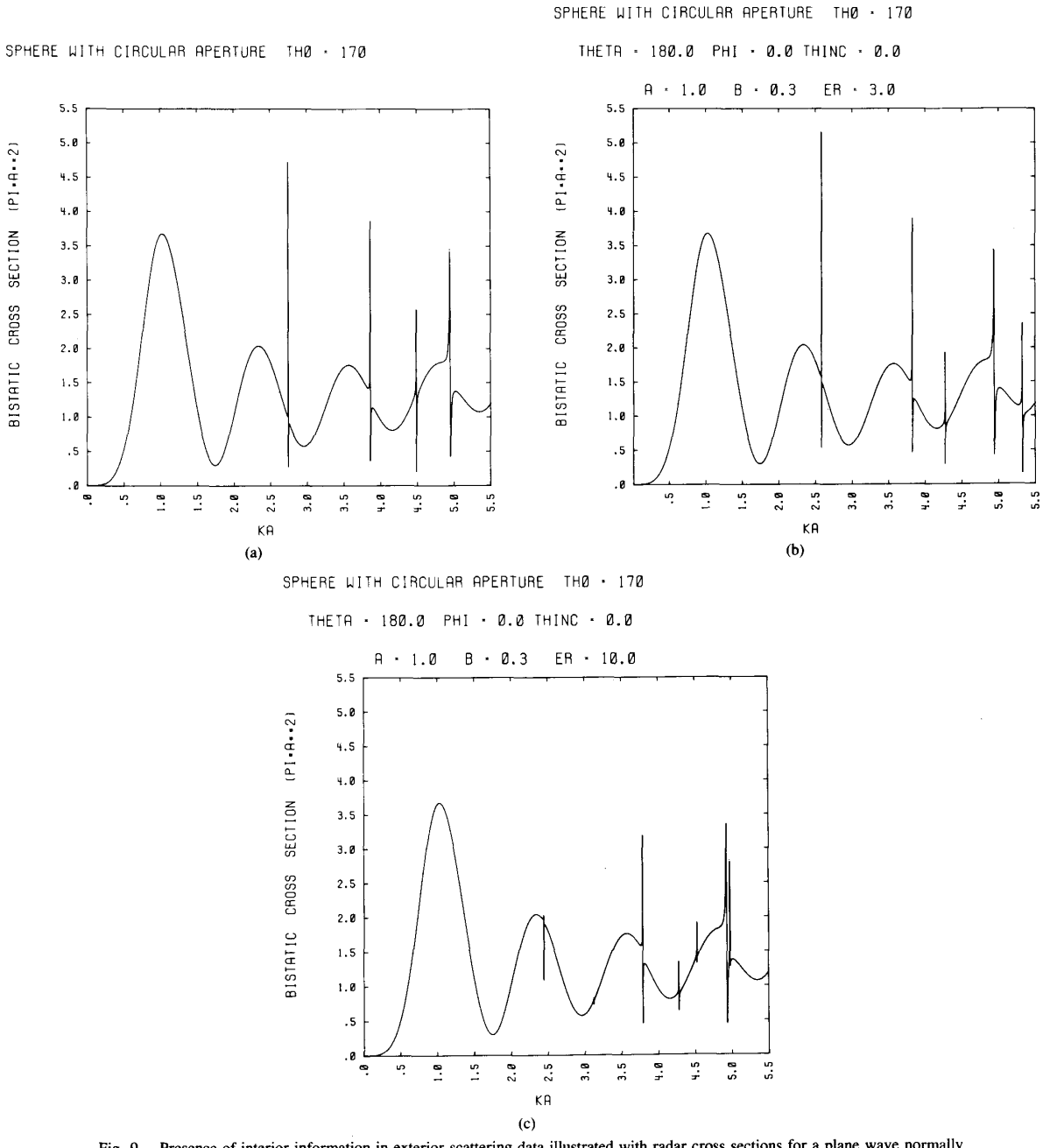

Fig. 9. Presence of interior information in exterior scattering data illustrated with radar cross sections for a plane wave normally incident into open spherical shells of radius a with a 10° aperture and enclosing concentric dielectric spheres with radius $b = 0.3a$. (a) Relative permittivity $\epsilon_r = 1.0$. (b) $\epsilon_r = 3.0$. (c) $\epsilon_r = 10.0$.

available cavity modes (hence CBA resonance features) becomes quite large as ka (frequency) increases.

This behavior of the resonances is explained by analyzing the migration of their locations in the closed-cavity case [13] and is illustrated in Figs. 10 and 11. The locations of the resonances are tracked for the corresponding closed metal exterior, $\epsilon_r = 3.0$ interior dielectric sphere case of Fig. 8 as a function of ka and the ratio b/a. As these figures indicate, there is a large variety of structures present in the mode spectrum for the closed cavity. This accounts for the different number of resonances in Fig. 8(a)–(d) for the cavity-backed aperture case and for the difference in their locations. The combination of knowing the location of the closed structure resonances and their anticipated presence in the exterior

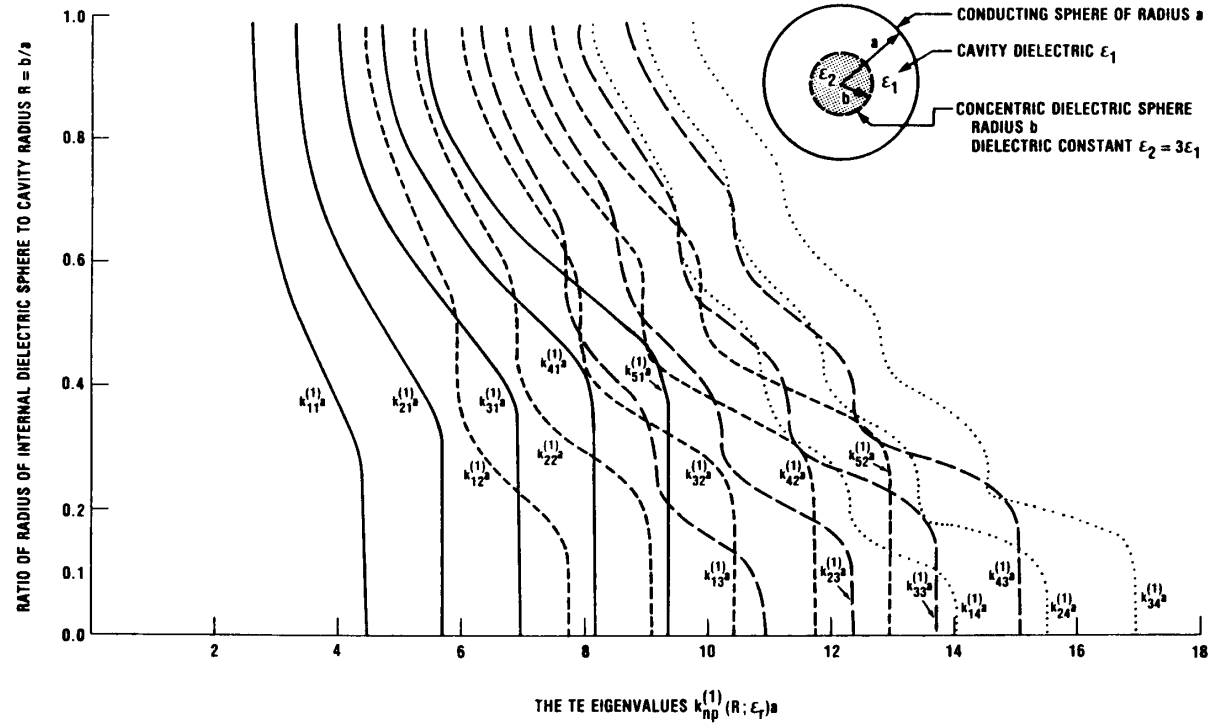

Fig. 10. Behavior of CBA resonance locations can be predicted by studying migration of eigenvalues in corresponding closed exterior sphere cases. Composite of trajectories of several TE eigenvalues for a spherical cavity of radius a internally loaded with a concentric dielectric sphere of radius b and relative permittivity $\epsilon_r = 3.0$ as the ratio b/a increases versus ka.

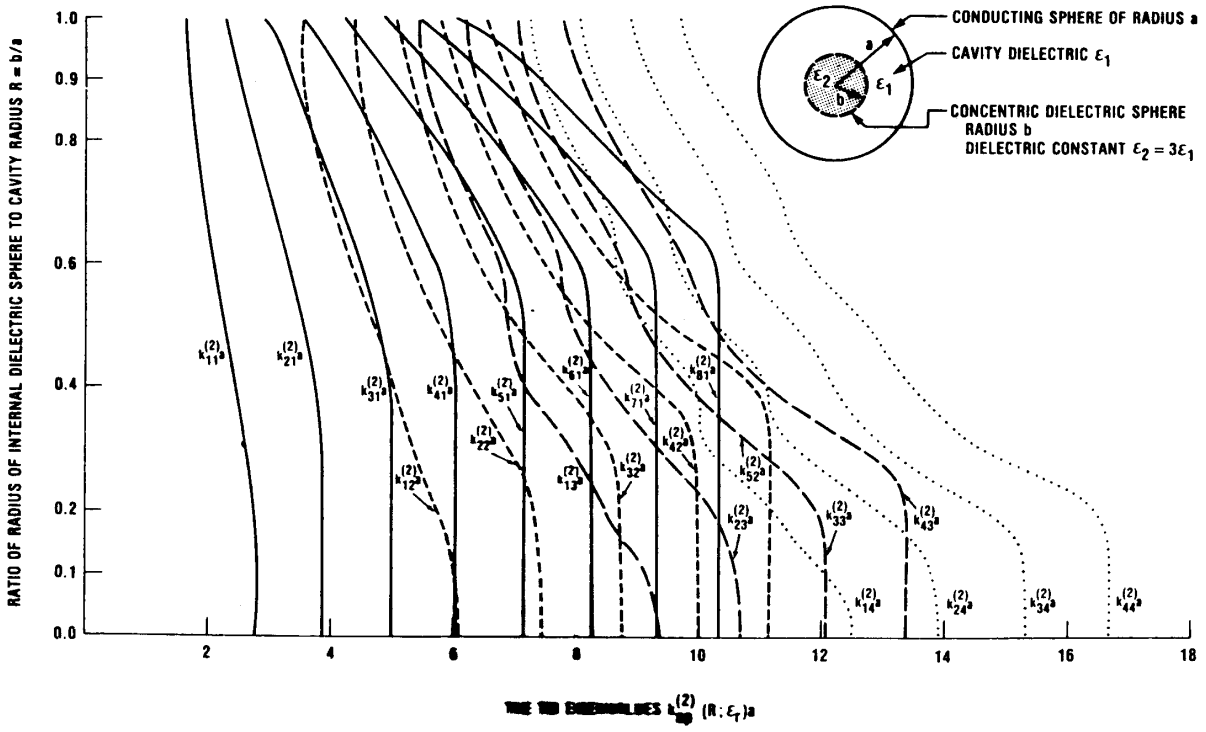

Fig. 11. Composite of corresponding trajectories of several TM eigenvalues for spherical cavity of radius a internally loaded with a concentric dielectric sphere of radius b and relative permittivity $\epsilon_r = 3.0$ as the ratio b/a increases versus ka.

scattering data has strong implications toward a potential object identification system and is currently being pursued.

IV. Discussion

Parameter studies of the generalized dual series solutions of several cavity-backed aperture canonical problems are enhancing our understanding of the aperture coupling and scattering processes. As shown here for the dielectrically loaded open sphere, the presence of the resonance features in the scattering cross sections are extremely interesting. The cross section resonances indicate that *for cavity-backed apertures there is interior information contained in the exterior scattering data.* The dependence of the location of these peaks on the interior structure and their presence at all look angles may have very important ramifications for diagnostic and object identification applications.

The antiresonance peaks in the empty open spherical shell and open cylinder radar cross sections have actually been observed experimentally [9], [10]. Nonetheless, for a lack of theoretical proof of their existence, they have been generally attributed to errors in the measurement apparatus [10]. The current analysis is but one attempt to overcome this situation and to make applied physicists as well as engineers aware of the new richness in studying cavity-backed aperture configurations.

References

[1] R. W. Ziolkowski, "*N*-series problems and the coupling of electromagnetic waves to apertures: A Riemann-Hilbert approach," *SIAM J. Math. Anal.*, vol. 16, no. 2, pp. 358-378, 1985.

[2] W. A. Johnson and R. W. Ziolkowski, "The scattering of an *H*-polarized plane wave from an axially slotted infinite cylinder: A dual series approach," *Radio Sci.*, vol. 19, no. 1, pp. 275-291, 1984.

[3] R. W. Ziolkowski, W. A. Johnson, and K. F. Casey, "Applications of Riemann-Hilbert problem techniques to electromagnetic coupling through apertures," *Radio Sci.*, vol. 19, no. 11, pp. 1425-1431, 1984.

[4] R. W. Ziolkowski and J. B. Grant, "Scattering from cavity-backed apertures: The generalized dual series solution of the concentrically loaded *E*-pol slit cylinder problem," *IEEE Trans. Antennas Propagat.*, vol. AP-35, no. 5, pp. 504-528, 1987.

[5] R. W. Ziolkowski and R. F. Schmucker, "Scattering from a slit cylinder enclosing an offset impedance surface," in *Proc. Nat. Radio Science Meeting*, Boulder, CO, URSI Paper B-8-8, Jan. 1986, p. 135.

[6] R. W. Ziolkowski and W. A. Johnson, "Electromagnetic scattering of an arbitrary plane wave from a spherical shell with a circular aperture," *J. Math. Phys.*, vol. 28, no. 6, pp. 1293-1314, 1987.

[7] R. W. Ziolkowski, "Scattering from a spherical shell with a circular aperture: cross-sections and energy storage for a normally incident plane wave," in *Proc. Nat. Radio Science Meeting*, Vancouver, BC, URSI Paper B-15-4, June 1985, p. 203.

[8] S. Chang and T. B. A. Senior, "Scattering by a spherical shell with a circular aperture," *AFWL Int. Notes*, Note 141, Apr. 1969.

[9] E. Garelis, "Initial heating rate of a droplet in a spherical microwave cavity," *Phys. Fluids*, vol. 17, no. 11, pp. 2002-2008, 1974.

[10] A. D. Steiger, "Electromagnetic eigenmode perturbations caused by deformation of a plasma core in a spherical cavity," *J. Math. Phys.*, vol. 18, no. 2, pp. 312-320, 1977.

[11] C. H. Woods, "Magnetohydrodynamic equilibrium of plasma confined in a spherical microwave cavity," *Phys. Fluids*, vol. 20, no. 2, pp. 252-258, 1977.

[12] D. L. Ensley, "Shape instability for a plasma contained within a standing electromagnetic field," *Phys. Fluids*, vol. 22, no. 12, pp. 2359-2363, 1979.

[13] L. F. Libelo, G. E. Pisane, and R. W. Ziolkowski, "Effects of dielectric loading on resonances in the concentric spherical cavity," in *Proc. Nuclear EMP Meeting*, Albuquerque, NM, Paper 104-7-5, May 1986, p. 147.

[14] R. W. Ziolkowski and W. A. Johnson, "Pseudo-decoupling Ansatz for electromagnetic aperture coupling," *Radio Sci.*, vol. 22, no. 2, pp. 169-174, 1987.

[15] K. F. Casey, "Quasi-static electric- and magnetic-field penetration of a spherical shield through a circular aperture," *IEEE Trans. Electromagn. Compat.*, vol. EMC-27, no. 1, pp. 13-17, 1987.

[16] R. W. Ziolkowski, "New electromagnetic resonance effects associated with cavity-backed apertures," *Radio Sci.*, vol. 22, no. 4, pp. 449-454, 1987.

Richard W. Ziolkowski (M'87), for a photograph and biography please see page 528 of the May 1987 issue of this TRANSACTIONS.

Diane P. Marsland (S'83-M'86) for a photograph and biography please see page 1444 of the December 1987 issue of this TRANSACTIONS.

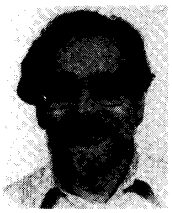

Louis F. Libelo, Jr. (M'76-SM'82) received the B.S. degree from Brooklyn College, Brooklyn, NY, in 1953, the M.S. degree from the University of Maryland, in 1956, and the Ph.D. degree from Rensselaer Polytechnic Institute, Troy, NY, in 1964, all in theoretical physics.

From 1956-1957 he worked for the Johns Hopkins University Operations Research Office. From 1958-1980 he conducted research on the theory of cooperative phenomena in materials and interaction of electromagnetic radiation with military systems at the Naval Surface Warfare Center, White Oaks, MD. From 1965-1971 he was a Professor of Physics at the American University, Washington, DC. He was an Adjunct Research Professor of Physics at the State University of New York, Albany in 1974-1978. He has been with the Harry Diamond Laboratories, Adelphi, MD, since 1980, conducting research in antenna theory, microwaves, and nuclear EMP. He is Group Leader of the HDL High Power Microwave source development and component technology research group.

Guy E. Pisane was born in Brooklyn, NY, on July 24, 1943. He received the B.S.E.E. degree in 1965, and the M.S. degree in electrophysics in 1968, both from the Polytechnic Institute of Brooklyn (now Polytechnic University of New York).

After further graduate studies, he worked for U.S. Government in both technical and nontechnical positions. He is currently an electronics engineer at Harry Diamond Laboratories, Adelphi, MD, where he has contributed to such areas as power generation, electromagnetic effects, and microwaves.